Spectra of Sparse Random Matrices

Reimer Kühn

Mathematics Department, King's College London, Strand, London WC2R 2LS,UK

26 March 2008

Abstract. We compute the spectral density for ensembles of of sparse symmetric random matrices using replica, managing to circumvent difficulties that have been encountered in earlier approaches along the lines first suggested in a seminal paper by Rodgers and Bray. Due attention is payed to the issue of localization. Our approach is not restricted to matrices defined on graphs with Poissonian degree distribution. Matrices defined on regular random graphs or on scale-free graphs, are easily handled. We also look at matrices with row constraints such as discrete graph Laplacians. Our approach naturally allows to unfold the total density of states into contributions coming from vertices of different local coordination.

1. Introduction

Since its inception by Wigner in the context of describing spectra of excited nuclei [1], Random Matrix Theory (RMT) has found applications in numerous areas of science, including questions concerning the stability of complex systems [2], electron localisation [3], quantum chaos [4], Quantum Chromo Dynamics [5], finance [6, 7], the physics of glasses both at elevated [8, 9] and low [10, 11] temperatures, number theory [12], and many many more. For an extensive review describing many of the applications in physics see, e.g. [13].

In the present paper we revisit the problem of determining the spectral density for ensembles of sparse random matrices pioneered two decades ago in seminal papers by Bray and Rodgers [14, 15]. The problem has in recent years received much renewed interest in connection with the study of complex networks, motivated, for instance, by the fact that geometric and topological properties of networks are reflected in spectral properties of adjacency matrices defining the networks in question [16, 17]. Also, phenomena such as non-exponential relaxation in glassy systems and gels [15, 18] — intimately related to Lifshitz tails [19] and Griffiths' singularities in disordered systems [20] — as well as

Anderson localization of electronic [21] or vibrational [22] states have been studied in sparsely connected random systems, as finite dimensional versions of these problems have proven to be extremely difficult to analyse. A wealth of analytical and numerical results has been accumulated on these systems in recent years. Progress has, however, been partly hampered by the fact that full solutions of the Rodgers-Bray integral equation [14], in terms of which spectral densities of the sparse random matrices in question are computed, have so far eluded us. Asymptotic analyses for large average connectivities [14, 15], and other approximation schemes such as the single defect approximation (SDA) and the effective medium approximation (EMA) [23, 24, 17] or very recently [25], as well as numerical diagonalization (e.g. [26]) had to come in for help.

In what follows we describe some significant progress in the understanding of this problem, based upon advances in the statistical mechanical analysis of sparsely connected spin-glass like systems seen in the last couple of years [27, 28] — in the present context in particular the proposal of a stochastic population-dynamics algorithm [28] to solve the nonlinear integral equations appearing in the solution of these problems, and the recent generalization of these methods to systems with continuous degrees of freedom, such as models of sparsely connected vector spins [29], or finitely coordinated models for low-temperature phases of amorphous systems [30].

It is well known that the average spectral density of an ensemble $\mathcal{M}$ of $N \times N$ matrices M can be computed from the ensemble average of the imaginary part of their resolvent via

$$\overline{\rho_N(\lambda)} = \frac{1}{\pi N}\mathrm{Im}\ \mathrm{Tr}\ \overline{\left[\lambda_\varepsilon \mathbb{1} - M\right]^{-1}}\ , \tag{1}$$

in which $\mathbb{1}$ is the $N \times N$ unit matrix, and $\lambda_\varepsilon = \lambda - i\varepsilon$, the limit $\varepsilon \to 0^+$ being understood. Following Edwards and Jones [31], one can express this result in terms of the Gaussian integral

$$Z_N = \int \prod_{i=1}^{N} \frac{\mathrm{d}u_i}{\sqrt{2\pi/i}}\ \exp\left\{ -\frac{i}{2}\sum_{i,j} u_i(\lambda_\varepsilon \delta_{ij} - M_{ij})u_j \right\} \tag{2}$$

as

$$\overline{\rho_N(\lambda)} = -\frac{2}{\pi N}\ \mathrm{Im}\ \frac{\partial}{\partial\lambda}\ \overline{\ln Z_N} = \frac{1}{N}\mathrm{Re}\ \sum_{i=1}^{N} \overline{\langle u_i^2 \rangle}\ , \tag{3}$$

using the replica method to evaluate the average of the logarithm in (3) over the ensemble $\mathcal{M}$ of matrices M under consideration. The 'averages' $\langle u_i^2 \rangle$ in (3) are evaluated with respect to the 'Gaussian measure' defined by (2).‡ This has been the path taken in [14]; we shall initially follow their reasoning.

‡ Note that we are using probabilistic notions in a loose, metaphorical sense, as the Gaussian measures used in these calculations are complex.

Disregarding the complex nature of the 'Hamiltonian' in the evaluation of (2), the mathematical problem posed in (2), (3) is analogous to the evaluation of an 'internal energy of a disordered system with quenched disorder. Within the general class of finitely coordinated amorphous model systems considered in [30], the one represented by (2), (3) constitutes a particular sub-class, viz. that of harmonically coupled systems, for which the analysis was found to be *much* simpler than for systems involving anharmonic couplings. Indeed, while the solution of the latter required the self-consistent determination of probability distributions over infinite dimensional function-spaces, it was realized in [30] that solutions of harmonically coupled systems could be formulated in terms of superpositions of Gaussians, and that the self-consistency problem reduced to the (much simpler) problem of a self-consistent determination of the probability distribution of their variances.

It can be fairly argued that this last insight is, in fact, easier to obtain within a Bethe-Peierls or cavity type approach [28], in which (2) is recursively evaluated *for given instances* on graphs which are locally tree-like, ignoring correlations among subtrees — an approximation that becomes exact, e.g., for random graphs that remain finitely coordinated in the thermodynamic limit. This approach is taken in a separate publication [32], in which (finite) single-instances and promising algorithmic aspects of the problem are being highlighted.

Although [30] describes all technical details needed for a replica analysis of the present problem, we shall nevertheless reproduce the key steps here, both to keep the paper self-contained, and to point out along the way where the impasse in [14] arises, and how it is circumvented.

The remainder of the paper is organized as follows. In Sec. 2, we describe the replica analysis of the problem posed by (2), (3), specializing to matrices defined on Poissonian (Erdös-Renyi) random graphs. It has been known for some time [31, 14] that the replica-symmetric high-temperature solution — i.e., a solution preserving both, permutation-symmetry among replica, and rotational symmetry in the space of replica — is exact for problems of the type considered here. Accordingly, a representation that respects these symmetries is formulated in Sec. 2.1. It is at this point where our formulation departs from that of [14]. In Sec. 3 we present results for a variety of examples, and compare with numerical diagonalization results for large finite matrices to assess their quality. In sufficiently sparse graphs, one expects localized states to appear. The signatures of localization within our approach are discussed throughout Sec. 3, with inverse participation ratios (IPRs) as a diagnostic tool looked at in Sec. 3.2. A detailed investigation of Anderson localization for (discrete) Schrödinger operators on sparse random graphs will be reserved to a separate publication [33]. Matrices with bimodal instead of Gaussian random couplings are studied in Sec. 3.3. As the formal structure of

the self-consistency problem remains unaltered when the Poissonian random graphs are replaced by graphs with other degree distributions [30], we can exploit this fact to present results for regular and scale-free random graphs in Sec. 3.4. Modifications needed to treat matrices with row-constraints, such as discrete graph Laplacians are outlined in Sec. 3.5. Our approach naturally allows to unfold the total density of states into contributions coming from vertices of different local coordination, and we finally present an example of such an unfolding in Sec. 3.6. The final Sec. 4 contains a brief summary and an outlook on promising directions for future research.

2. Replica Analysis

2.1. General Formulation

Here we briefly outline the evaluation of (2), (3) for sparse symmetric matries M of the form

$$M_{ij} = c_{ij} K_{ij} \ , \tag{4}$$

in which $C = \{c_{ij}\}$ is a symmetric adjacency matrix of an undirected random graph (with $c_{ii} = 0$), and the non-zero elements of M are specified by the K_{ij}, also taken to be symmetric in the indices. Within the present outline we restrict ourselves for the sake of simplicity to adjacency matrices of Erdös-Renyi random graphs, with

$$P(\{c_{ij}\}) = \prod_{i<j} p(c_{ij}) \delta_{c_{ij},c_{ji}} \qquad \text{and} \qquad p(c_{ij}) = \left(1 - \frac{c}{N}\right) \delta_{c_{ij},0} + \frac{c}{N} \delta_{c_{ij},1} \ ,$$

exhibiting a Posisssonian degree distribution with average coordination c. We note at the outset that formal results carry over without modification to other cases [30]. There is no need at this point to specify the distribution of the K_{ij}, but we shall typically look at Gaussian and bimodal distributions.

The average (3) is evaluated using replica $\overline{\ln Z_N} = \lim_{n\to 0} \frac{1}{n} \ln \overline{Z_N^n}$, starting with integer numbers of replica as usual. After performing the average over the distribution of the connectivities one obtains

$$\overline{Z_N^n} = \int \prod_{ia} \frac{\mathrm{d}u_{ia}}{\sqrt{2\pi/i}} \exp\left\{ -\frac{i}{2} \lambda_\varepsilon \sum_{i,a} u_{ia}^2 + \frac{c}{2N} \sum_{ij} \left(\left\langle \exp\left(iK \sum_a u_{ia} u_{ja} \right) \right\rangle_K - 1 \right) \right\} \ , \tag{5}$$

in which $\langle \ldots \rangle_K$ refers to an average over the distribution of the K_{ij}. A decoupling of sites is achieved by introducing the replicated density

$$\rho(\boldsymbol{u}) = \frac{1}{N} \sum_i \prod_a \delta\Big(u_a - u_{ia}\Big) \ , \tag{6}$$

with $\boldsymbol{u}$ denoting the replica vector $\boldsymbol{u} = (u_1, u_2, \ldots, u_n)$, and enforcing its definition via functional δ distributions,

$$1 = \int \mathcal{D}\rho\mathcal{D}\hat{\rho}\ \exp\left\{-i\int \mathrm{d}\boldsymbol{u}\hat{\rho}(\boldsymbol{u})\Big(N\rho(\boldsymbol{u}) - \sum_i \prod_a \delta\Big(u_a - u_{ia}\Big)\Big)\right\}\ . \tag{7}$$

This gives (using shorthands of the form $\mathrm{d}\rho(\boldsymbol{u}) \equiv \mathrm{d}\boldsymbol{u}\rho(\boldsymbol{u})$ where useful)

$$\begin{aligned}\overline{Z_N^n} \quad &= \int \mathcal{D}\rho \int \mathcal{D}\hat{\rho}\ \exp\left\{N\left[\frac{c}{2}\int \mathrm{d}\rho(\boldsymbol{u})\mathrm{d}\rho(\boldsymbol{v})\left(\left\langle \exp\left(iK\sum_a u_a v_a\right)\right\rangle_K - 1\right)\right.\right. \\ &\left.\left. - \int \mathrm{d}\boldsymbol{u}\, i\hat{\rho}(\boldsymbol{u})\rho(\boldsymbol{u}) + \ln\int\prod_a \frac{\mathrm{d}u_a}{\sqrt{2\pi/i}} \exp\left(i\,\hat{\rho}(\boldsymbol{x}) - \frac{i}{2}\lambda_\varepsilon \sum_a u_a^2\right)\right]\right\}\ ,\end{aligned} \tag{8}$$

allowing to evaluate $N^{-1}\ln\overline{Z_N^n}$ by a saddle point method. The stationarity conditions w.r.t. variations of ρ and $\hat{\rho}$ read

$$i\hat{\rho}(\boldsymbol{u}) = c\int \mathrm{d}\rho(\boldsymbol{v})\left(\left\langle \exp\left(iK\sum_a u_a v_a\right)\right\rangle_K - 1\right)\ , \tag{9}$$

$$\rho(\boldsymbol{u}) \ = \frac{\exp\left(i\,\hat{\rho}(\boldsymbol{u}) - \frac{i}{2}\lambda_\varepsilon \sum_a u_a^2\right)}{\int \mathrm{d}\boldsymbol{u}\exp\left(i\,\hat{\rho}(\boldsymbol{u}) - \frac{i}{2}\lambda_\varepsilon \sum_a u_a^2\right)}\ . \tag{10}$$

The way in which sites are decoupled constitutes the first point of departure between our treatment and that of [14] and subsequent analyses inspired by it (e.g. [34, 35]). In these papers the averaged exponential expressions in the exponent of (5),

$$f(\boldsymbol{u}_i\cdot\boldsymbol{v}_j) = f\Big(\sum_a u_{ia}v_{ja}\Big) = \left\langle \exp\left(iK\sum_a u_{ia}v_{ja}\right)\right\rangle_K - 1\ , \tag{11}$$

is expanded, and an infinite family of multi-replica generalizations of Edwards Anderson order parameters (and corresponding Hubbard-Stratonovich transformations) are used to decouple the sites, much as in the treatment of the dilute spin-glass problem by Viana and Bray [36]. The authors then use the expansion and the infinite set of self-consistency equations for the multi-replica generalizations of Edwards Anderson order parameters to construct a non-linear integral equation for a function g defined via a suitable 'average' of f; see [14] for details. Our treatment in this respect is closer in spirit to the alternative approach of Kanter and Sompolinsky [37] who treat local field distributions (which in the general context of disordered amorphous systems discussed in [30] become distributions of local potentials) as the primary object of their theory.

However, the difference between our treatment and that of [14] is at this point still superficial. Indeed, we have the correspondence

$$i\hat{\rho}(\boldsymbol{u}) = cg(\boldsymbol{u}) \tag{12}$$

between our 'conjugate density' $\hat{\rho}$ and the function g of [14]. With this identification, (9) and (10) can be combined to give

$$g(\boldsymbol{u}) = \frac{\int \mathrm{d}\boldsymbol{v}\ f(\boldsymbol{u}\cdot\boldsymbol{v})\ \exp\left(cg(\boldsymbol{v}) - \frac{i}{2}\lambda_\varepsilon \boldsymbol{v}^2\right)}{\int \mathrm{d}\boldsymbol{v}\ \exp\left(cg(\boldsymbol{v}) - \frac{i}{2}\lambda_\varepsilon \boldsymbol{v}^2\right)} \ , \tag{13}$$

which is the Rodgers-Bray integral equation for general distributions of non-zero bond strengths.

2.2. Replica Symmetry

To deal with the $n \to 0$ limit in these equations, assumptions concerning the invariance properties of the solutions $\rho(\boldsymbol{u})$ and $\hat{\rho}(\boldsymbol{u})$ of (9) and (10) — alternatively of the solution $g(\boldsymbol{u})$ of (13)— under transformations among the replica are required. It has been established for some time [31, 14] that the replica-symmetric high-temperature solution — i.e., a solution preserving both, permutation-symmetry among replica, and rotational symmetry in the space of replica — is exact for problems of the type considered here. It is here where the paths taken in the present paper and in [14] really bifurcate. In [14], the assumption $g(\boldsymbol{u}) = g(u)$, with $u = |\boldsymbol{u}|$ is used to perform the angular integrals in n-dimensional polar coordinates in (13), resulting in an integral equation for $g(u)$ in the $n \to 0$-limit. This integral equation has also been obtained using the supersymmetry approach [38]. It has, however, so far resisted exhaustive analysis or full numerical solution.

In the present paper we follow [30], and represent ρ and $\hat{\rho}$ as superpositions of replica-symmetric functions, using the observation made in [30] that superpositions of Gaussians of the form

$$\rho(\boldsymbol{u}) \ = \int \mathrm{d}\pi(\omega) \prod_a \frac{\exp\left[-\frac{\omega}{2}u_a^2\right]}{Z(\omega)} \ , \tag{14}$$

$$i\hat{\rho}(\boldsymbol{u}) = \hat{c} \int \mathrm{d}\hat{\pi}(\hat{\omega}) \prod_a \frac{\exp\left[-\frac{\hat{\omega}}{2}u_a^2\right]}{Z(\hat{\omega})} \ , \tag{15}$$

would provide exact solutions for harmonically coupled systems. Note that these expressions do indeed preserve permutation symmetry among replica as well as rotational symmetry. In (15) the constant $\hat{c}$ is to be determined such that $\hat{\pi}$ is normalized, $\int \mathrm{d}\hat{\pi}(\hat{\omega}) = 1$. We note that these representations make sense only for $\mathrm{Re}\ \omega > 0$ and $\mathrm{Re}\ \hat{\omega} > 0$; later on we shall find that these conditions are self-consistently met for solutions of the fixed point equations. Expressing (8) in terms of π and $\hat{\pi}$, we get

$$\overline{Z_N^n} = \int \mathcal{D}\pi\mathcal{D}\hat{\pi} \exp\left\{N\left[G_1[\pi] + G_2[\hat{\pi},\pi] + G_3[\hat{\pi}]\right]\right\} \ . \tag{16}$$

As $n \to 0$, the functionals G_1, G_2 and G_3 evaluate to

$$G_1[\pi] \quad \simeq n\frac{c}{2}\int \mathrm{d}\pi(\omega)\mathrm{d}\pi(\omega') \ \left\langle \ln \frac{Z_2(\omega,\omega',K)}{Z(\omega)Z(\omega')} \right\rangle_K \ , \tag{17}$$

$$G_2[\hat{\pi},\pi] \simeq \ -\hat{c} - n\hat{c}\int \mathrm{d}\hat{\pi}(\hat{\omega})\mathrm{d}\pi(\omega) \ \ln \frac{Z(\hat{\omega}+\omega)}{Z(\hat{\omega})Z(\omega)} \ , \tag{18}$$

$$G_3[\hat{\pi}] \quad \simeq \hat{c} + n\sum_{k=0}^{\infty} p_{\hat{c}}(k)\int \{\mathrm{d}\hat{\pi}\}_k \ \ln \frac{Z_\lambda(\{\hat{\omega}\}_k)}{\prod_{\ell=1}^k Z(\hat{\omega}_\ell)} \ , \tag{19}$$

in which we have introduced the shorthands $\{\mathrm{d}\hat{\pi}\}_k \equiv \prod_{\ell=1}^k \mathrm{d}\hat{\pi}(\hat{\omega}_\ell)$, and $\{\hat{\omega}\}_k = \sum_{\ell=1}^k \hat{\omega}_\ell$, a Poissonian connectivity distribution

$$p_{\hat{c}}(k) = \frac{\hat{c}^k}{k!}\exp[-\hat{c}] \tag{20}$$

with average connectivity $\langle k\rangle = \hat{c}$, and the 'partition functions'

$$Z(\omega) \qquad = \int \mathrm{d}u \ \exp\left[-\frac{\omega}{2}u^2\right] = \sqrt{2\pi/\omega} \ , \tag{21}$$

$$Z_{\lambda_\varepsilon}(\{\hat{\omega}\}_k) \quad = \int \frac{\mathrm{d}u}{\sqrt{2\pi/i}} \ \exp\left[-\frac{1}{2}\Big(i\lambda_\varepsilon + \{\hat{\omega}\}_k\Big)u^2\right] = \left(\frac{i}{i\lambda_\varepsilon + \{\hat{\omega}\}_k}\right)^{1/2} \ , \tag{22}$$

$$Z_2(\omega,\omega',K) = \int \mathrm{d}u\mathrm{d}v \ \exp\left[-\frac{1}{2}\Big(\omega u^2 + \omega' v^2 - 2iKuv\Big)\right] = \frac{2\pi}{\sqrt{\omega\omega' + K^2}} \ . \tag{23}$$

Note that the $\mathcal{O}(1)$ contributions of G_2 and G_3 in the exponent of (8) cancel in their sum.

The stationarity condition of the functional integral (8) w.r.t variations of ρ and $\hat{\rho}$ is reformulated in terms of stationarity conditions w.r.t variations π and $\hat{\pi}$,

$$\hat{c}\int \mathrm{d}\hat{\pi}(\hat{\omega})\ln\frac{Z(\hat{\omega}+\omega)}{Z(\hat{\omega})Z(\omega)} = c\int \mathrm{d}\pi(\omega')\left\langle \ln\frac{Z_2(\omega,\omega',K)}{Z(\omega)Z(\omega')}\right\rangle_K + \mu \ , \tag{24}$$

$$\hat{c}\int \mathrm{d}\pi(\omega)\ln\frac{Z(\hat{\omega}+\omega)}{Z(\hat{\omega})Z(\omega)} = \sum_{k\geq 1} kp_{\hat{c}}(k)\int \{\mathrm{d}\hat{\pi}\}_{k-1}\ln\frac{Z_{\lambda_\varepsilon}(\hat{\omega}+\{\hat{\omega}\}_{k-1})}{Z(\hat{\omega})\prod_{\ell=1}^{k-1}Z(\hat{\omega}_\ell)} + \hat{\mu} \ , \tag{25}$$

with μ and $\hat{\mu}$ Lagrange multipliers to take the normalization of π and $\hat{\pi}$ into account.

The conditions that (24) must hold for all ω and similarly that (25) must hold for all $\hat{\omega}$ can be translated [28] into

$$\hat{\pi}(\hat{\omega}) = \frac{c}{\hat{c}}\int \mathrm{d}\pi(\omega') \ \left\langle \delta(\hat{\omega} - \hat{\Omega}(\omega',K))\right\rangle_K \ , \tag{26}$$

$$\pi(\omega) = \sum_{k\geq 1}\frac{k}{\hat{c}}p_{\hat{c}}(k)\int \{\mathrm{d}\hat{\pi}\}_{k-1} \ \delta\left(\omega - \Omega(\{\hat{\omega}\}_{k-1})\right) \ , \tag{27}$$

in which $\hat{\Omega}(\omega',K)$ and $\Omega(\{\hat{\omega}\}_{k-1})$ are defined via

$$Z(\omega + \hat{\Omega}(\omega',K)) = \frac{Z_2(\omega,\omega',K)}{Z(\omega')} \qquad \Leftrightarrow \qquad \hat{\Omega}(\omega',K) = \frac{K^2}{\omega'} \ , \tag{28}$$

and

$$\Omega(\{\hat{\omega}\}_{k-1}) = i\lambda_\varepsilon + \sum_{\ell=1}^{k-1} \hat{\omega}_\ell \ , \tag{29}$$

respectively. Given that π is normalized, it follows from (26) that the same is true for $\hat{\pi}$, provided $\hat{c} = c$, so the fixed point equations take their final form as

$$\hat{\pi}(\hat{\omega}) = \int \mathrm{d}\pi(\omega') \ \left\langle \delta(\hat{\omega} - \hat{\Omega}(\omega', K)) \right\rangle_K \ , \tag{30}$$

$$\pi(\omega) = \sum_{k\geq 1} \frac{k}{c} p_c(k) \int \{\mathrm{d}\hat{\pi}\}_{k-1} \ \delta\left(\omega - \Omega(\{\hat{\omega}\}_{k-1})\right) \ . \tag{31}$$

These equations can be seen as special cases of the general framework derived in [30], when restricted to harmonically coupled random systems. In [30] it is shown that they hold — unmodified — for non-Poissonian degree distributions as well, as long as the average connectivity in these systems remains finite.

Note that for all $\varepsilon > 0$, π and $\hat{\pi}$ — self-consistently — have support in Re $\omega > 0$ and Re $\hat{\omega} > 0$ as required. The equations take a form that suggests solving them via a stochastic population-based algorithm, as described in Appendix A.

For the thermodynamic limit of the spectral density we obtain from (2), (3) and (16)-(23) that

$$\begin{aligned}\overline{\rho(\lambda)} &= \frac{1}{\pi} \mathrm{Im} \sum_{k=0}^{\infty} p_c(k) \int \{\mathrm{d}\hat{\pi}\}_k \ \frac{i}{i\lambda_\varepsilon + \{\hat{\omega}\}_k} \\ &= \frac{1}{\pi} \sum_{k=0}^{\infty} p_c(k) \int \{\mathrm{d}\hat{\pi}\}_k \ \frac{\mathrm{Re}(\{\hat{\omega}\}_k + \varepsilon)}{\left(\mathrm{Re}(\{\hat{\omega}\}_k + \varepsilon)\right)^2 + \left(\lambda + \mathrm{Im}\,\{\hat{\omega}\}_k\right)^2} \ .\end{aligned} \tag{32}$$

This expression has a natural interpretation as a sum of contributions of local-densities of state of sites with connectivities k, weighted according to their probability of occurrence. Referring to (3), we may further identify the

$$\sigma_k^2 = \frac{1}{\pi} \mathrm{Im} \ \frac{i}{i\lambda_\varepsilon + \{\hat{\omega}\}_k} \tag{33}$$

as realizations of the variance of (Gaussian) marginals on sites of coordination k.

With an eye towards disentangling singular (pure point) and continuous contributions to the spectral density, we find it useful to define

$$P(a,b) = \sum_k p_c(k) \int \{\mathrm{d}\hat{\pi}\}_k \ \delta\left(a - \mathrm{Re}\ \{\hat{\omega}\}_k\right) \delta\left(b - \mathrm{Im}\ \{\hat{\omega}\}_k\right) \ , \tag{34}$$

with $a \geq 0$ by construction. The density of states can then be expressed as an integral over P,

$$\overline{\rho(\lambda)} = \int \frac{\mathrm{d}a \ \mathrm{d}b}{\pi} \ P(a,b) \ \frac{a + \varepsilon}{(a+\varepsilon)^2 + (b+\lambda)^2} \ . \tag{35}$$

Noting the singlular nature of the above integrand in the limit $\varepsilon \to 0$ for $a = 0$, we propose to isolate possible singular contributions to the spectral density by writing

$$P(a,b) = P_0(b)\delta(a) + \tilde{P}(a,b)\ . \tag{36}$$

This gives

$$\overline{\rho(\lambda)} = \int \mathrm{d}b\ P_0(b)\mathcal{L}_\varepsilon(b+\lambda) + \int_{a>0} \frac{\mathrm{d}a\ \mathrm{d}b}{\pi}\ \tilde{P}(a,b)\ \frac{a+\varepsilon}{(a+\varepsilon)^2+(b+\lambda)^2}\ , \tag{37}$$

in which $\mathcal{L}_\varepsilon$ denotes a Lorentzian of width ε. Our results below strongly suggest that, when the limit $\varepsilon \to 0$ is taken — thereby $\mathcal{L}_\varepsilon(x) \to \delta(x)$ — a non-zero value of

$$P_0(-\lambda) = \lim_{\varepsilon\to 0} \int \mathrm{d}b\ P_0(b)\mathcal{L}_\varepsilon(b+\lambda) \tag{38}$$

gives the contribution of the pure-point spectrum, originating from localized states, to the overall spectral density.

This concludes the general framework.

3. Results

In what follows, we report results for a variety of different ensembles of sparse random matrices, in order to explore the capabilities and limitations of our approach. In order to properly appreciate the results presented below, it is worth pointing out that within our stochastic population-dynamics based approach to solving the fixed point equations (30) and (31), the integrals (32), or (35), (37) are evaluated by *sampling* from a population. Denoting by $\mathcal{N}$ the number of samples (a_i, b_i) taken, we have, e.g.,

$$\overline{\rho(\lambda)} \simeq \frac{1}{\mathcal{N}} \left[\sum_{\substack{i=1\\ a_i=0}}^{\mathcal{N}} \mathcal{L}_\varepsilon(b_i+\lambda) + \frac{1}{\pi} \sum_{\substack{i=1\\ a_i>0}}^{\mathcal{N}} \frac{a_i+\varepsilon}{(a_i+\varepsilon)^2+(b_i+\lambda)^2} \right] \tag{39}$$

as an approximation of (37). The $\varepsilon \to 0$-limit is clearly singular in the first contribution to (39). If $b_i + \lambda \neq 0$ for all b_i in the sample, one obtains zero in the $\varepsilon \to 0$-limit, whereas one obtains a diverging contribution, if $b_i + \lambda = 0$ for at least one b_i in the sample. The second alternative will quite generally be an event of probability zero, so a small regularizing $\varepsilon > 0$ must be kept in order to 'see' this contributions (if it exists). In what follows, we shall refer to the two contributions to (37), as $\overline{\rho_s(\lambda)}$ and $\overline{\rho_c(\lambda)}$, with

$$\overline{\rho_s(\lambda)} \simeq \frac{1}{\mathcal{N}} \sum_{\substack{i=1\\ a_i=0}}^{\mathcal{N}} \mathcal{L}_\varepsilon(b_i+\lambda)\ , \quad \overline{\rho_c(\lambda)} \simeq \frac{1}{\pi\mathcal{N}} \sum_{\substack{i=1\\ a_i>0}}^{\mathcal{N}} \frac{a_i+\varepsilon}{(a_i+\varepsilon)^2+(b_i+\lambda)^2}\ . \tag{40}$$

The population-dynamics algorithm itself is run with a small regularizing $\varepsilon > 0$ (as required in (2) to guarantee existence of the integral). While running the algorithm, we use $\varepsilon = 10^{-300}$, which is close to the smallest representable real number in double-precision arithmetic on the machines used for the numerics.

3.1. Poisson Random Graphs — Gaussian Couplings

Our first results pertain to sparse matrices defined on Poisson random graphs, with Gaussian couplings. The left panel of Fig. 1 shows spectral densities for the case of mean connectivity $c = 4$, having Gaussian random couplings with $\langle K_{ij}^2 \rangle = 1/c$. For this system we find an integrable power-law divergence of the form

$$\overline{\rho}(\lambda) \simeq 0.05|\lambda|^{-0.61} \; , \qquad \lambda \to 0 \; , \tag{41}$$

and a δ peak at $\lambda = 0$, the latter originating from isolated sites in the ensemble. Results of numerical diagonalizations (using a sample of 500 $N \times N$ matrices with $N = 2000$ are shown for comparison, and the agreement is excellent.

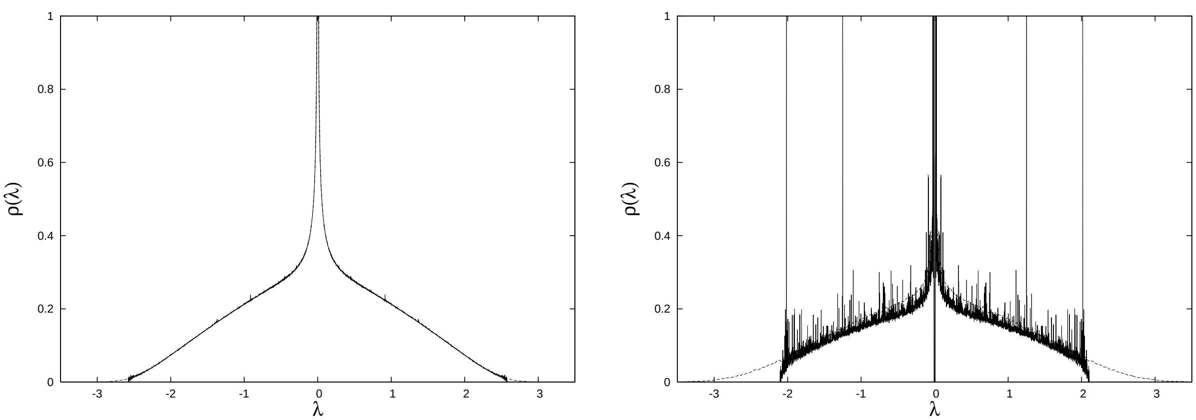

Figure 1. Spectral density for matrices defined on Poissonian random graphs with $c = 4$ (left panel) and $c = 2$ (right panel), having Gaussian random couplings with $\langle K_{ij}^2 \rangle = 1/c$. Full line: results obtained from the present theory; dashed line: results obtained from a sample of 2000×2000 matrices. In both cases $\varepsilon = 10^{-300}$ was used in the evaluation of (39).

The behaviour changes rather drastically if the average connectivity is reduced to $c = 2$ — a value closer to the percolation threshold $c_c = 1$. In this case the spectral density shows strong fluctuations, when evaluated with the same small regularizer. These originate from $\overline{\rho_s}$ in (40), and are related to the pure point spectrum associated with localized eigenstates coming from a collection of isolated finite clusters of all sizes in the ensemble. These exist for $c = 4$ as well, but their contribution is too small to be easily notable when

combined with $\overline{\rho_c}$ in (39). In addition, there is a central δ peak as in the $c = 4$-case which appears to be separated from the main bands by a gap; see the second panel in Fig 2. The agreement with results of numerical diagonalization is fairly poor as it stands; in particular, exponential tails of localized states extending beyond the apparent edge of the central band are missed in this way. However, when (39) is evaluated with a regularizing $\varepsilon = 10^{-3}$ comparable to the resolution of the λ-scan, the agreement is once more excellent as shown in Fig 2. It is worth noting in this context that numerical simulations, in which binning of eigenvalues is used to determine the the spectral density *also imply a form of regularization*, and they do not distinguish continuous and singular contributions to the DOS if the distribution of the singular contributions is itself reasonably uniform.

When displayed on a logarithmic scale, the results clearly reveal two interesting features: (i) a localization transition at $\lambda_c \simeq 2.295$, characterised by a vanishing continuous contribution $\overline{\rho_c}$ to (39) for $|\lambda| > \lambda_c$, and (ii) exponential (Lifshitz) tails [19] in the spectral density, related to localized states represented by the singular contribution $\overline{\rho_s}$ to (39)), and exhibited only through regularization. We shall substantiate this analysis in the following sub-section by looking at the behaviour inverse participation ratios. The same phenomena are seen for $c = 4$, where $\lambda_c \simeq 2.581$.

3.2. Inverse Participation Ratios and Localization

In order to substantiate our identification of singular and continuous contributions to the spectral densities we look at Inverse Participation Ratios (IPRs) of eigenstates as obtained from numerical diagonalizations. Given eigenvectors $\boldsymbol{v}$ of a (random) matrix, their IPRs are defined as

$$\mathrm{IPR}(\boldsymbol{v}) = \frac{\sum_{i=1}^N v_i^4}{\left(\sum_{i=1}^N v_i^2\right)^2} \ . \tag{42}$$

As eigenvectors can always be chosen to be normalized, we see that IPRs remain of order 1 for localized states which have a few $\mathcal{O}(1)$ eigenvector components — the extreme case being $\mathrm{IPR}(\boldsymbol{v}) = 1$ for $v_i = \delta_{i,i_0}$ — whereas they are $\mathcal{O}(N^{-1})$ for fully extended states for which $v_i = \mathcal{O}(N^{-1/2})$ for all i.

Here we only produce a qualitative comparison for the two cases studied in the previous subsection, comparing IPRs computed for systems of size $N = 100$ and $N = 1000$, and using scatter-plots of IPRs vs eigenvalues to exhibit the salient features. As clearly visible, there remains a substantial fraction of states at all λ in the $c = 2$ case, which do *not* exhibit the N^{-1} scaling of IPRs expected for delocalized states; the tails, and a small central band in particular appear to be *dominated* by localized states. By contrast in the $c = 4$ case there is a notable depletion of states with $\mathcal{O}(1)$ IPRs, except for $\lambda = 0$ and in the tails of

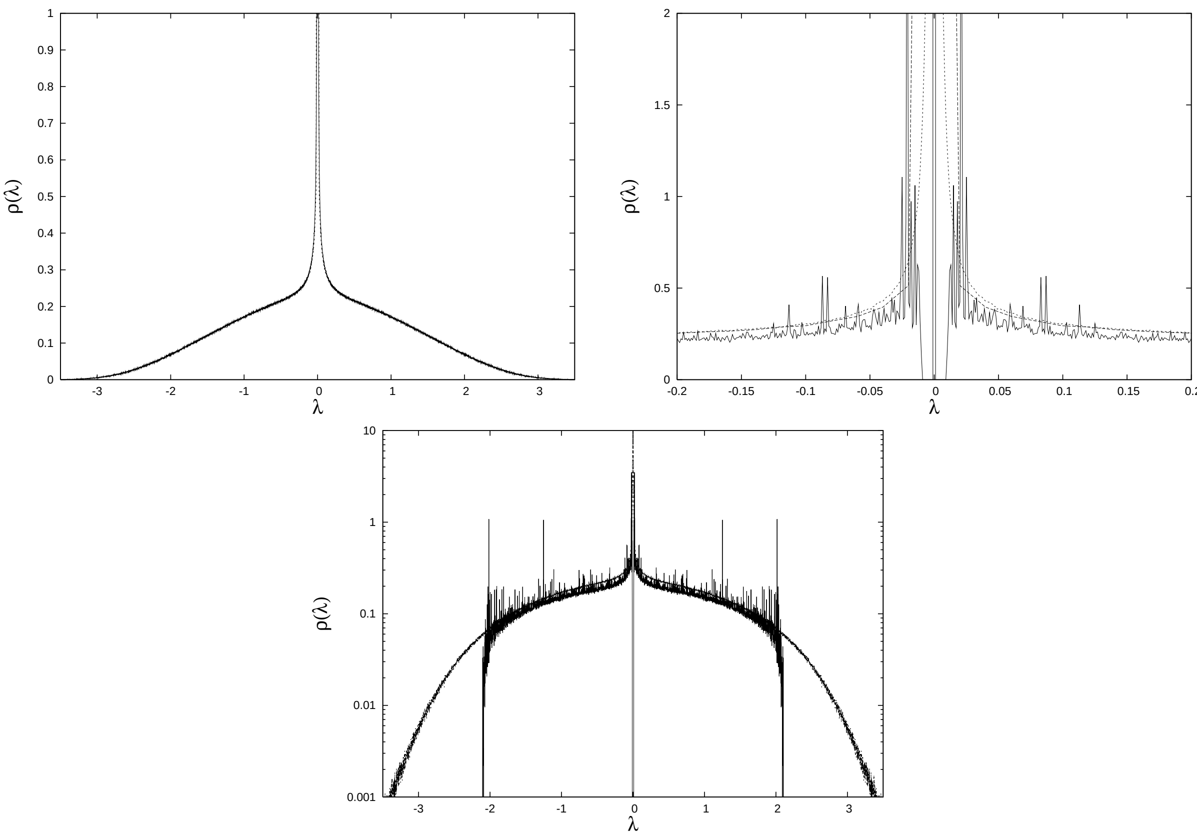

Figure 2. Upper left panel: Spectral density for matrices defined on Poissonian random graphs with $c = 2$ as in the previous figure, but now evaluated with a regularizing $\varepsilon = 10^{-3}$ in (39) (full line). At the resolution given the result is indistinguishable from the numerical simulation results (dashed line). Upper right panel: zoom into the central region comparing results obtained with the small regularizer, exhibiting a gap around the central peak (full line), with a larger regularizer $\varepsilon = 10^{-3}$ (short dashed line) and with results of numerical diagonalization (long dashed line). The same comparison is made in the lower panel for a larger portion of the spectrum on a logarithmic scale. The regularized $\varepsilon = 10^{-3}$-results are on this scale indistinguishable from those of the numerical simulations. Note the localization transition and the Lifshitz tails as discussed in the main text.

the spectrum. These findings are entirely consistent with our identifications made in the previous subsection. We note that the role of regularization in identifying localized states has been pointed out before using heuristics related to the evaluation of *local* densities of state [22].

We shall return to this issue in greater quantitative detail in a separate paper devoted to Anderson localization in discrete random Schrödinger operators defined on sparse random graphs [33].

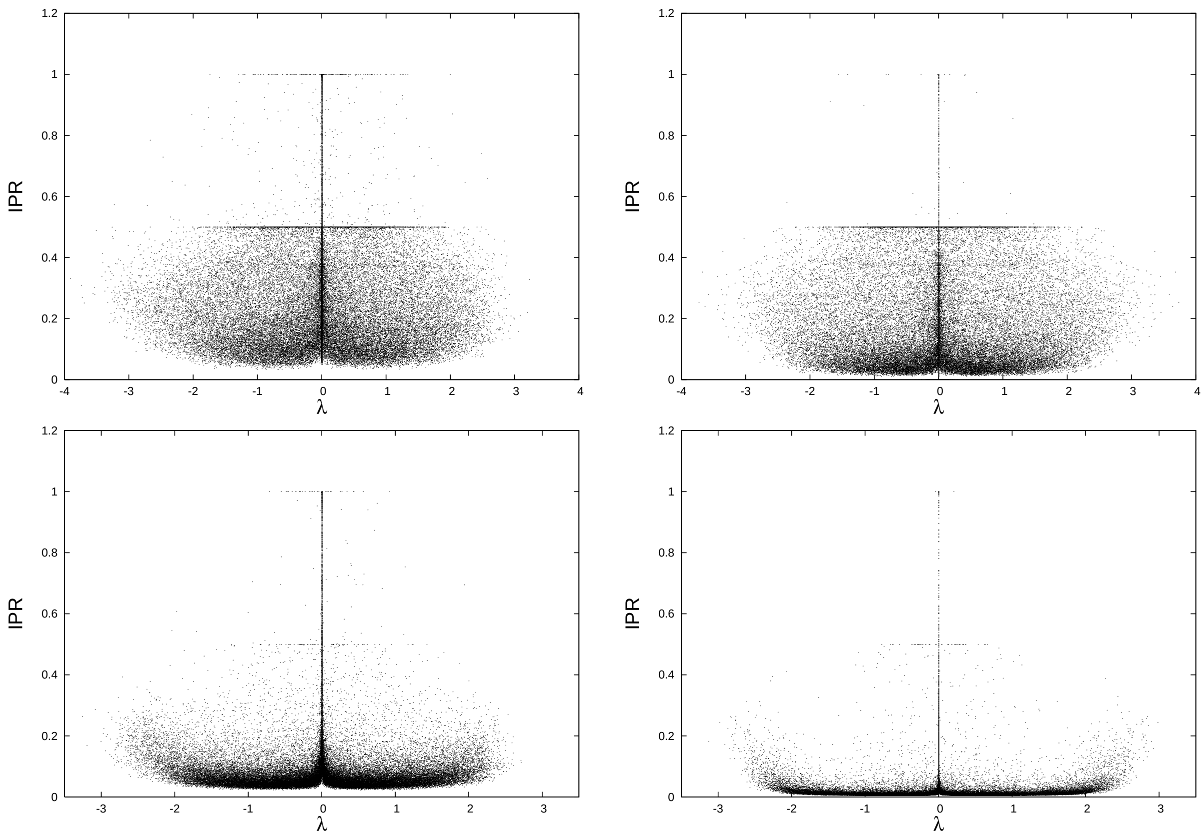

Figure 3. Scatterplots showing eigenvalue against IPRs for Poissonian random graphs with $c = 2$ (first row) and $c = 4$ (second row). The graphs in the left column correspond to $N = 100$, those in the right column to $N = 1000$.

3.3. Poisson Random Graphs — Bimodal Couplings

We can also look at coupling distributions different from Gaussian for the non-zero couplings, e.g. fixed $K_{ij} = 1/\sqrt{c}$ or bi-modal $K_{ij} = \pm 1/\sqrt{c}$. As noted before [14], both give rise to the same spectral densities on large sparse (tree-like) graphs due to the absence of frustrated loops. It can also be seen as a consequence of the appearance of K^2 in (28).

We choose a Poissonian random graph *at* the percolation threshold $c = 1$ as an example that allows us to highlight both the strengths and the limitations of the present approach. It is known that all states will be localized for this system. In Fig 4 we compare results of a λ-scan with resolution $\delta\lambda = 10^{-3}$, using a regularizer $\varepsilon = 10^{-4}$ for the scan. The smaller panels exhibit numerical diagonalization results, as well as a comparison between the two using a zoom into the region around $\lambda = 1$.

On the side of the strengths, we note that the spectral density obtained from our algorithm is able to display more details than can be exposed by simulation results obtainable at

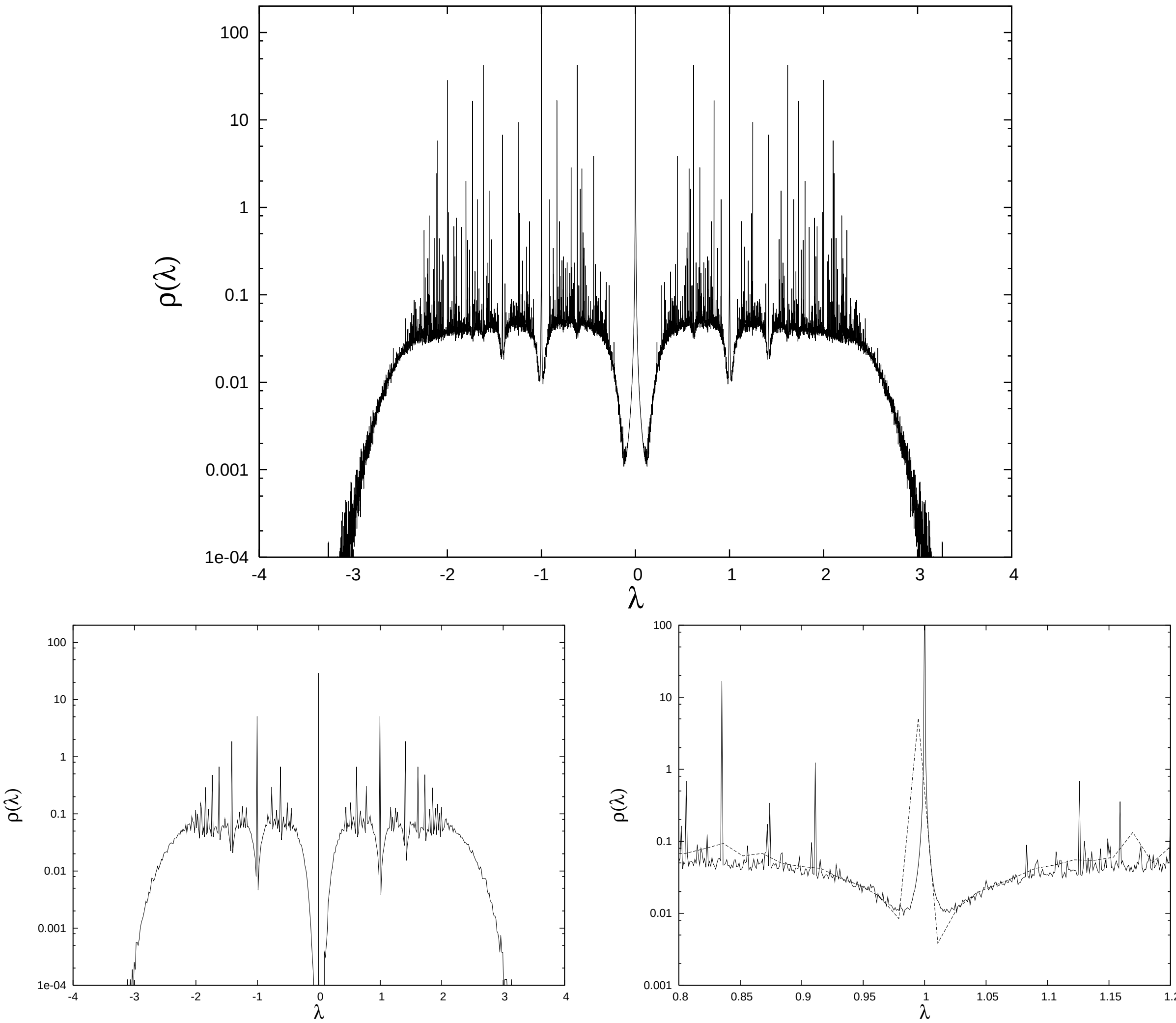

Figure 4. Comparison of spectral density for $K_{ij} = \pm 1/\sqrt{c}$, on a Poissonian random graph with $c = 1$ as computed via the present algorithm (main panel) with results from numerical diagonalisation of $N \times N$ matrices of the same type with $N = 2000$ (lower left) and a direct comparison in the region around $\lambda = 1$.

reasonable effort. On the downside, one might note that the results for this system attain the status of semi-quantitative results, as they do depend on the chosen regularization, though in fairness it should be said that the same applies to the results obtained via numerical diagonalization where results vary with the binning resolution. In the present case this is due to the fact that the spectrum for most parts consists of a dense collection of δ peaks [39]. A notable deficiency is the broadening of delta-peaks into Lorentzians of finite width, which creates artefacts around isolated delta-peaks, exemplified here by the peak at $\lambda = 0$. Since the origin of this deficiency is understood, more precise details can, if desired, be recovered by choosing a smaller regularizing ε.

3.4. Regular and Scale-Free Random Graphs

In the present section we consider matrices defined on regular and scale-free random graphs.

3.4.1. Regular Random Graphs Our theory applies unmodified to matrices defined on graphs with degree distributions other than Poissonian, as long as the *mean connectivity remains finite*. We use this fact to obtain spectra of matrices with Gaussian random couplings defined on regular random graphs with fixed connectivity c, choosing $\langle K_{ij}^2 \rangle = 1/c$ for the couplings. Results for $c = 4$ and $c = 100$ are shown in Fig. 5. The $c = 4$ results are compared with simulations, with results analogous to previous cases, including the presence of a localization transition at $\lambda_c \simeq 2.14$

The second example is chosen as a test to see the semicircular law [40] reemerge in the limit of large (though finite) connectivity. This limit can also be extracted from the fixed point equations. It is somewhat easier to verify for results pertaining to single instances [32] than for the ensemble.

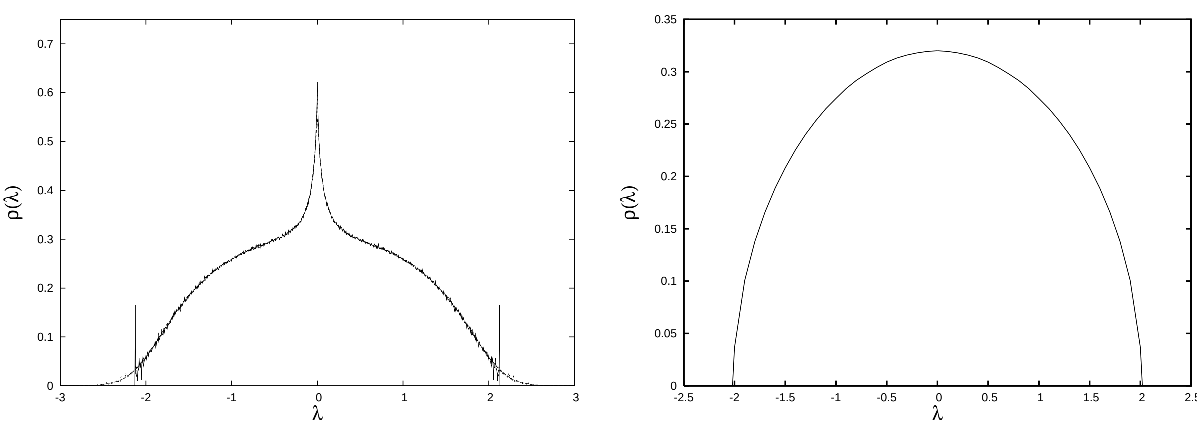

Figure 5. Spectral densities for a random graph with fixed connectivity $c = 4$ (left), and on a random graph with fixed non-random connectivity $c = 100$ (right).

3.4.2. Scale-Free Graphs We have also looked at a scale free graph with connectivity distribution given by $p(k) = P_0 k^{-\gamma}$ with $\gamma = 4$ and a lower cut-off at $k = 2$. Results shown in Fig. 6 reveal a continuous central band, and localized states for $|\lambda| > \lambda_c \simeq 2.85$ much as in the other cases. For the present system, the tails in the spectral density follow a power law of the form $\rho(\lambda) \sim \lambda^{1-2\gamma}$ [17, 41].

Comparison with exact diagonalization results is facilitated by a fast algorithm that allows to generate sparse graphs with arbitrary degree distribution [42].

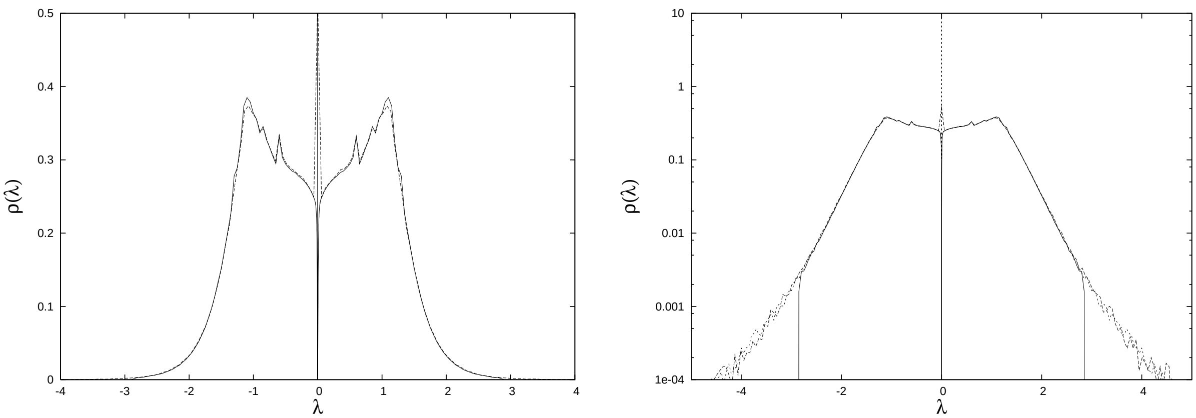

Figure 6. Spectral density for for $K_{ij} = \pm 1/\sqrt{c}$ on a random graph with power-law degree distribution of average connectivity $c \simeq 2.623$. Left panel: results obtained with small regularizer (full line), and numerical diagonalization results from a sample of 500 matrices of dimension $N = 2000$ (dashed line). Right panel: the same results displayed on a logartithmic scale, this time with results regularized at $\varepsilon = 10^{-3}$ (short dashed line) included.

3.5. Graph Laplacians

Let us finally look at matrices row-constraints, such as related to discrete graph-Laplacians.

The discrete graph Laplacian of a graph with connectivity matrix $C = \{c_{ij}\}$ has matrix elements

$$\Delta_{ij} = c_{ij} - \delta_{ij} \sum_k c_{ik} \ . \tag{43}$$

A quadratic form involving the Laplacian can be written in the form

$$\frac{1}{2} \sum_{ij} \Delta_{ij} u_i u_j = -\frac{1}{4} \sum_{ij} c_{ij} (u_i - u_j)^2 \ . \tag{44}$$

As before we shall be interested in more general matrices with zero row-sum constraint of the form

$$M_{ij} = c_{ij} K_{ij} - \delta_{ij} \sum_k c_{ik} K_{ij} \ . \tag{45}$$

To evaluate the spectral density within the present framework one would thus have to compute

$$\overline{Z_N^n} = \int \prod_{ia} \frac{\mathrm{d}u_{ia}}{\sqrt{2\pi/i}} \exp\left\{ -\frac{i}{2} \lambda_\varepsilon \sum_{i,a} u_{ia}^2 + \frac{c}{2N} \sum_{ij} \left(\left\langle \exp\left(\frac{iK}{2} \sum_a (u_{ia} - u_{ja})^2 \right) \right\rangle_K - 1 \right) \right\}$$

instead of (5). The required modification has, of course, been noted earlier [15, 43]. The resulting problem constitutes precisely (the harmonic variant of) the translationally invariant systems, for which the framework in [30] was developed in the first place. The general theory can be copied word for word, and the fixed point equations (30), (31) remain formally unaltered except for the change in $Z_2(\omega, \omega', K)$ in (23), owing to the modified interaction term, which gives rise to a modified expression for $\hat{\Omega}(\omega', K)$ in (28). We obtain

$$\hat{\Omega}(\omega', K) = \frac{K\omega'}{K - i\omega'} \tag{46}$$

instead of (28). Fig. 7 shows the spectrum of a Laplacian for a Posisson random graph with $c = 2$, comparing our solution (upper left panel) computed with $\varepsilon = 10^{-3}$ with numerical diagonalization results in the upper right panel. We use $K_{ij} \equiv 1/c$ for the non-zero matrix elements in this case. As in the other cases, we observe a localization transition, here at $\lambda_c \simeq -3.98$. Results obtained with a small regularizer $\varepsilon = 10^{-300}$ exhibiting only the continuous part of the spectrum are shown in the lower panel.

3.6. Unfolding Spectral Densities

As a last item in this study we look at the possibility of unfolding the spectral density according to contributions of local densities of state, coming from vertices of different coordination, as suggested by Eq. (32). This method has been used in [30] to look at distributions of Debye-Waller factors in amorphous systems, unfolded according to local coordinations. In the present context it may provide an interesting diagnostic tool to help understanding localization phenomena.

Fig 8 exhibits the spectrum of the graph Laplacian shown in the previous figure along with its unfolding into contributions of local densities of state with different coordination. The present example clearly shows that — somewhat paradoxically — the well connected sites are the ones providing the dominant contributions to localized states in the lower band-edge Lifshitz tails. The clearly identifiable humps in the figure correspond from left to right to $k = 9$, $k = 8$, $k = 7$, $k = 6$, $k = 5$, $k = 4$, and $k = 3$, which easily allows to identify the corresponding contributions to the spectral density, the contribution of $k = 2$ gives rise to several notable humps in the spectral density, and together with the $k = 1$ contribution is mainly responsible for the dip at $\lambda = -1$. The $k = 0$ contribution is mainly responsible for the δ-peak at $\lambda = 0$ (which is broadenend into a Lorentzian of width $\varepsilon = 10^{-3}$ due to the regularization, as discussed earlier.

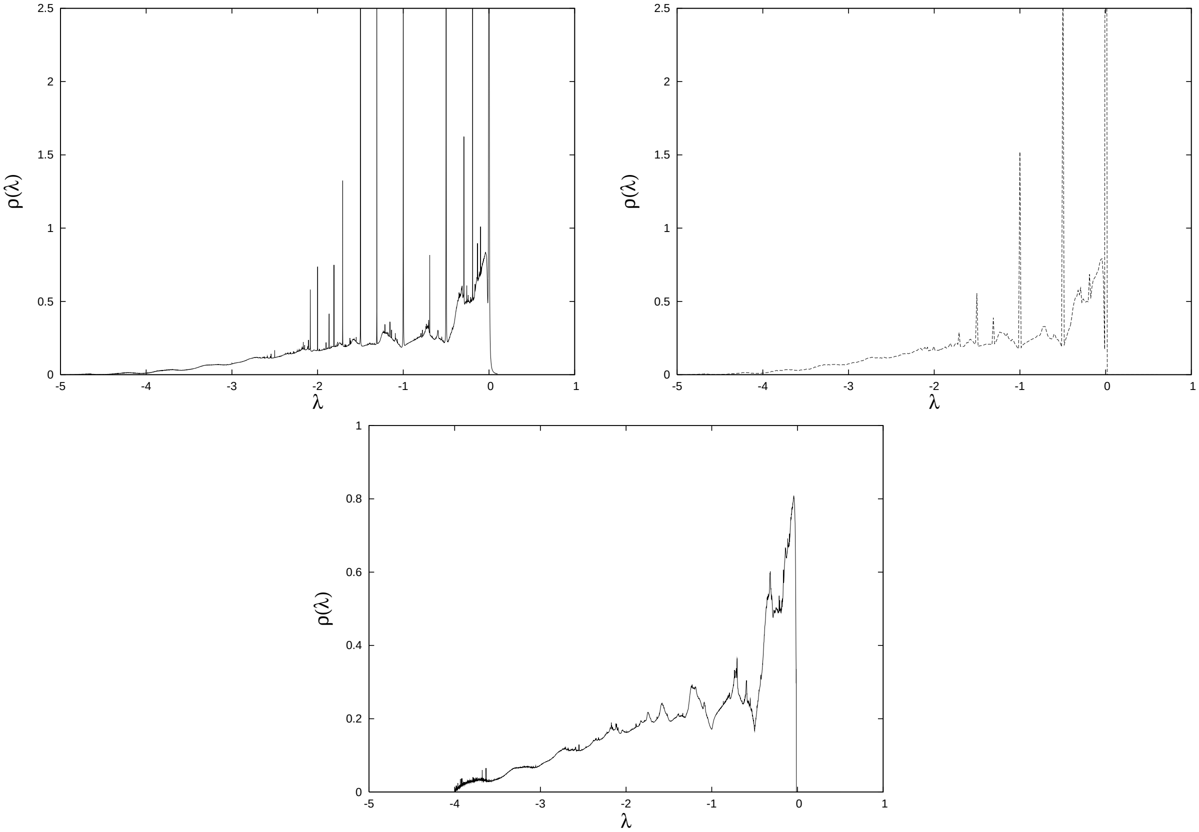

Figure 7. Spectral density for the Laplacian on a Poissonian random graph with $c = 2$ as computed via the present algorithm. Upper left panel: $\varepsilon = 10^{-3}$-results; upper right panel: results from numerical diagonalisation of $N \times N$ matrices of the same type with $N = 2000$. Lower panel: continuous part of the spectrum obtained using $\varepsilon = 10^{-300}$ as a regularizer.

4. Conclusions

In the present paper we have used a reformulation of the replica approach to the computation of spectral densities for sparse matrices, which allows to obtain spectral densities in the thermodynamic limit to any desired detail — limited only by computational resources. Our method is versatile in that it allows to study systems with arbitrary degree distributions, as long as they give rise to connectivity distributions with finite mean. A cavity approach that emphasises results on finite instances will appear elsewhere [32]. As expected (and well known), the Wigner semi-circle reemerges in the large c limit as discussed in [32]. Large and small λ asymptotics remain to be investigated. Our method allows to expose the separate contributions of localized and extended states to the spectral density, and thereby to study localization transitions. We shall explore this issue in greater detail in a separate publication. Indeed, with results for graph-Laplacians

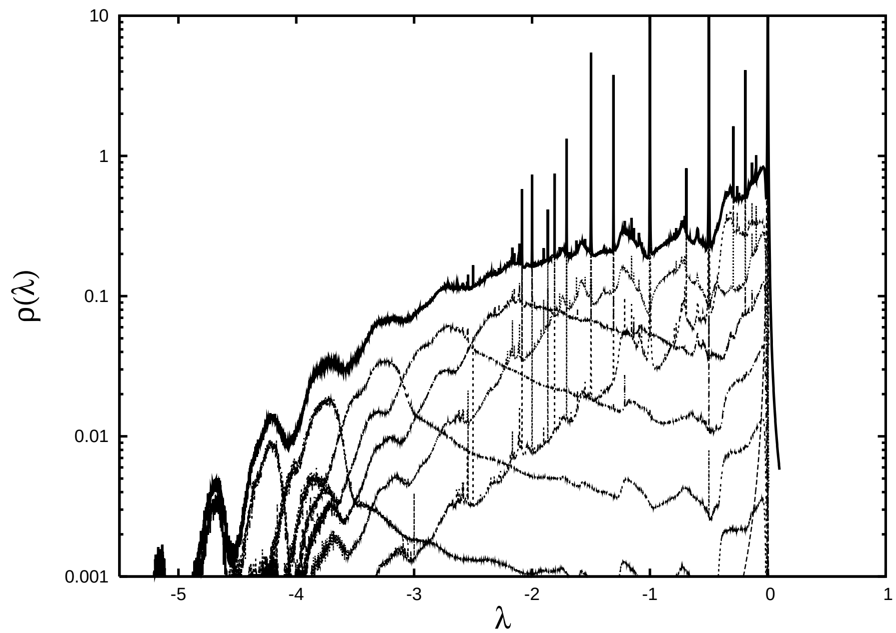

Figure 8. Spectral density for the Laplacian on a Poissonian random graph with $c = 2$ (full upper line), shown together with its unfolding according to contributions of different coordination, as discussed in the main text.

in hand, the step towards a study of discrete random Schrödinger operators and Anderson localization in such systems is just around the corner [33]. A generalization to asymmetric matrices using both the cavity method and a replica approach for the ensemble along the lines of [44] is currently under investigation in our group [45]. Other problems we have started to look at are spectra of modular systems [46] and small world networks.

We believe our results to constitute an improvement over previous asymptotic results as well as over results obtained by closed form approximations. They may open the way to further interesting lines of research. Let us here mention just a few such examples: within RMT proper, one might wish to further investigate the degree of universality of level correlations in these systems [47]; one could refine the random matrix analysis of financial cross-correlations [7] by taking non-trivial degree distributions of economic interactions into account, or one might wish to look at finite connectivity variants of random reactance networks [48], taking e.g. regular connectivity 4 to compare with results of numerical simulations of such systems on two-dimensional square lattices.

Acknowledgements It is a pleasure to thank Güler Ergün, Jort van Mourik, Isaac Pérez-Castillo, Tim Rogers and Koujin Takeda for illuminating discussions. Jort van Mourik also kindly supplied instances of scale free-random graphs to allow comparison of ensemble results and results from numerical diagonalization in this case.

Appendix A. Population Dynamics

The stochastic algorithm used to solve (30), (31) takes the following form. Populations $\{\omega_i; 1 \leq i \leq N_p\}$ and $\{\hat{\omega}_i; 1 \leq i \leq N_p\}$ are randomly initialized with Re $\omega_i > 0$ and Re $\hat{\omega}_i > 0$.

Then the following steps are iterated

1. Generate a random $k \sim \frac{k}{c} p_c(k)$.

2. Randomly select $k-1$ elements from $\{\hat{\omega}_i; 1 \leq i \leq N_p\}$; compute

$$\Omega = i\lambda_\varepsilon + \sum_{j=1}^{k-1} \hat{\omega}_{i_j} \ , \tag{A.1}$$

and replace ω_i by Ω for a randomly selected $i \in \{1, \ldots, N_p\}$.

3. Select $j \in \{1, \ldots, N_p\}$ at random, generate a random K according to distribution of bond strengths; compute

$$\hat{\Omega} = \frac{K^2}{\omega_j} \qquad , \qquad \left(\text{or} \quad \hat{\Omega} = \frac{K\omega_j}{K - i\omega_j} \quad \text{for zero row-sums} \right) , \tag{A.2}$$

and replace $\hat{\omega}_i$ by $\hat{\Omega}$ for a randomly selected $i \in \{1, \ldots, N_p\}$.

4. return to **1.**

This algorithm is iterated until populations with stable distributions of $\{\hat{\omega}_i; 1 \leq i \leq N_p\}$ and $\{\omega_i; 1 \leq i \leq N_p\}$ are attained.

A variant of this algorithm when implemented on instances of real graphs generates the belief-propagation or cavity equations for this problem, as studied in [32]. It can be derived directly in terms iterative evaluations of (2) on locally tree-like graphs.

References

[1] E. P. Wigner. On the Statistical Distribution of the Widths and Spacings of Nuclear Resonance Levels. *Proc. Cambr. Philos. Soc.*, 47:790–798, 1951.

[2] R. M. May. Will a Large Complex System be Stable? *Nature*, 238:413–414, 1972.

[3] D. J. Thouless. Maximum Metallic Resistance in Thin Wires. *Phys. Rev. Lett.*, 39:1167–1169, 1977.

[4] O. Bohigas, M. J. Giannoni, and C. Schmit. Characterization of Chaotic Quantum Spectra and Universality of Level Fluctuation Laws. *Phys. Rev. Lett.*, 52:1–4, 1984.

[5] J. Verbaarschot. The Spectrum of the QCD Dirac Operator and Chiral Random Matrix Theory: The Threefold Way. *Phys. Rev. Lett.*, 72:2531–2533, 1994.

[6] L. Laloux, P. Cizeau, J.-P. Bouchaud, and M. Potters. Noise Dressing of Financial Correlation Matrices. *Phys. Rev. Lett.*, 83:1467–1470, 1999.

[7] V. Plerou, P. Gopikrishnan, B. Rosenow, L. A. N. Amaral, and H. E. Stanley. Universal and Non-Universal Properties of Cross-Correlations in Financial Time Series. *Phys.Rev. Lett.*, 83:1471–1474, 1999.

[8] A. Cavagna, I. Giardina, and G. Parisi. Analytic Computation of the Instantaneous Normal Modes Spectrum in Low Density Liquids. *Phys. Rev. Lett.*, 83:108–111, 1999.

[9] K. Broderix, K.K. Bhattacharya, A. Cavagna, A. Zippelius, and I. Giardina. Saddles on the Potential Energy Landscape of a Lennard-Jones Liquid. *AIP Conf. Proceedings*, 553:23–27, 2001.

[10] R. Kühn and U. Horstmann. Random Matrix Approach to Glassy Physics: Low Temperatures and Beyond. *Phys. Rev. Lett.*, 78:4067–4070, 1997.

[11] R. Kühn. Universality in Glassy Low-Temperature Physics. *Europhys. Lett.*, 62:313–319, 2003.

[12] J.P. Keating and N.C. Snaith. Random Matrix Theory and L-Functions at $s = 1/2$. *Comm. Math. Phys.*, 214:91–110, 2000.

[13] T. Guhr, A. Müller-Groeling, and H. A. Weidenmüller. Random Matrix Theories in Quantum Physics: Common Concepts. *Phys. Rep.*, 299:190–425, 1998.

[14] G. J. Rodgers and A. J. Bray. Density of States of a Sparse Random Matrix. *Phys. Rev. B*, 37:3557–3562, 1988.

[15] A. J. Bray and G. J. Rodgers. Diffusion in a Sparsely Connected Space: A Model for Glassy Relaxation. *Phys. Rev. B*, 38:11461–11470, 1988.

[16] R. Albert and A.-L. Barabási. Statistical Mechanics of Complex Networks. *Rev. Mod. Phys.*, 74:47–97, 2002.

[17] S. N. Dorogovtsev, A. V. Goltsev, J. F. F. Mendes, and A. N. Samukhin. Spectra of Complex Networks. *Phys. Rev. E*, 68(4):046109, 2003.

[18] K. Broderix, T. Aspelmeyer, A.K. Hartmann, and A. Zippelius. Stress Relaxation of Near-Critical Gels. *Phys. Rev. E*, 64:021404, 2001.

[19] O. Khorunzhiy, W. Kirsch, and P. Müller. Lifshitz Tails for Spectra of Erdös-Renyi Random Graphs. *Ann. Appl. Prob.*, 16:295–309, 2006, arXiv:math-ph/0502054.

[20] R. B. Griffiths. Nonanalytic Behavior Above the Critical Point in a Random Ising Ferromagnet. *Phys. Rev. Lett.*, 23:17–19, 1969.

[21] S. N. Evangelou. Spectral Density Singularities, Level Statistics. and Localization in a Sparse Random Matrix Ensemble. *Phys. Rev. Lett*, 68:361–364, 1992.

[22] S. Ciliberti, T. S. Grigera, V. Martín-Mayor, G. Parisi, and P. Verrocchio. Anderson Localization in Euclidean Random Matrices. *Phys. Rev. B*, 71:153104, 2005.

[23] G. Biroli and R. Monasson. A Single Defect Approximation for Localized States on Random Lattices. *J. Phys. A*, 32:L255–L261, 1999.

[24] G. Semerjian and L. F. Cugliandolo. Sparse Random Matrices: The Eigenvalue Spectrum Revisited. *J. Phys. A*, 35:4837–4851, 2002.

[25] T. Nagao and G. J. Rodgers. Spectral Density of Complex Networks with a Finite Mean Degree. arXiv:cond-mat/08031042, 2008.

[26] K.-I. Goh, B. Kahng, and D. Kim. Spectra and Eigenvectors of Scale-Free Networks. *Phys. Rev. E*, 64:051903, 2001.

[27] R. Monasson. Optimization Problems and Replica Symmetry Breaking in Finite Connectivity Spin-Glasses. *J. Phys. A*, 31:513–529, 1998.

[28] M. Mézard and G. Parisi. The Bethe Lattice Spin Glass Revisited. *Eur. Phys. J. B*, 20:217–233, 2001.

[29] A.C.C. Coolen, N S Skantzos, I. Pérez-Castillo, C .J. Pérez-Vicente, J. P. L. Hatchett, B. Wemmenhove, and T. Nikoletopoulos. Finitely Connected Vector Spin Systems with Random Matrix Interactions. *J. Phys. A*, 38:8289–8317, 2005.

[30] R. Kühn, J. van Mourik, M. Weigt, and A. Zippelius. Finitely Coordinated Models for Low-Temperature Phases of Amorphous Systems. *J. Phys. A*, 40:9227–9252, 2007.

[31] S. F. Edwards and R. C. Jones. The Eigenvalue Spectrum of a Large Symmetric Random Matrix. *J. Phys. A*, 9:1595–1603, 1976.

[32] T. Rogers, I. Pérez-Castillo, R. Kühn, and K. Takeda. Cavity Approach to the Spectral Density of Sparse Symmetric Random Matrices. *arXiv:cond-mat/0803.1553*, 2008.

[33] R. Kühn and J. van Mourik. Localization in Random-Schrödinger Operators on Sparse Random Graphs . *work in progres*, 2008.

[34] G. J. Rodgers, K. Austin, B. Kahng, and D. Kim. Eigenvalue Spectra of Complex Networks. *J. Phys. A*, 38:9431–9437, 2005.

[35] D. Kim and B. Kahng. Spectral densities of scale-free networks. arXiv:cond-mat/0703055.

[36] L.Viana and A.J. Bray. Phase Diagrams for Dilute Spin Glasses. *J. Phys. C*, 18:3037–3051, 1985.

[37] I. Kanter and H. Sompolinsky. Mean-Field Theory of Spin-Glasses with Finite Ccoordination Number. *Phys. Rev. Lett.*, 58:164–167, 1987.

[38] Y. V. Fyodorov and A. D. Mirlin. On the Density of States of Sparse Random Matrices. *J. Phys. A*, 24:2219–2223, 1991.

[39] O. Golinelli. Statistics of Delta Peaks in the Spectral Density of Large Random Trees. *arXiv:cond-mat/0301437*, 2003.

[40] E. P. Wigner. On the Distribution of the Roots of Certain Symmetric Matrices. *Ann. Math.*, 67:325–327, 1958.

[41] M. Mihail and C. Papadimitriou. On the Eigenvalue Power Law. *Lect. Notes Comput. Sci.*, 2483:254–262, 2002.

[42] J. van Mourik and Y. Kabashima. The Polynomial Error Probability for LDPC Codes. arXiv:cond-mat/0310177, 2003.

[43] J. Stäring, B. Mehlig, Y. V. Fyodorov, and J. M. Luck. Random symmetric Matrices with a Constraint: The Spectral Density of Random Impedance Networks. *Phys. Rev. E*, 67:047101, 2003.

[44] F. Haake, F. Izrailev, N. Lehmann, D. Saher, and H.-J. Sommers. Statistics of Complex Levels of Random Matrices for Decaying Systems. *Z. Phys. B*, 88:359–370, 1992.

[45] K. Anand and T. Rogers. work in progress. 2008.

[46] G. Ergün and R. Kühn. Spectra of Sparsely Connected Modular Random Matrices. *to be published*, 2008.

[47] A. D. Mirlin and Y. V. Fyodorov. Universality of Level Correlation Function of Sparse Random Matrices. *J. Phys. A*, 24:2273–2286, 1991.

[48] Y. V. Fyodorov. Spectral Properties of Random Reactance Networks and Random Matrix Pencils. *J. Phys. A*, 32:7429–7446, 1999.